Using Nitrile Functional Groups to Replace Amines for Solution-Deposited Single-Walled Carbon Nanotube Network Films

Justin P. Opatkiewicz, Melburne C. LeMieux, Derrick Liu, Michael Vosgueritchian, Soumendra N. Barman, Claire M. Elkins, James Hedrick, and Zhenan Bao*

Department of Chemical Engineering, Stanford University, Stanford, California 94305, United States

ABSTRACT

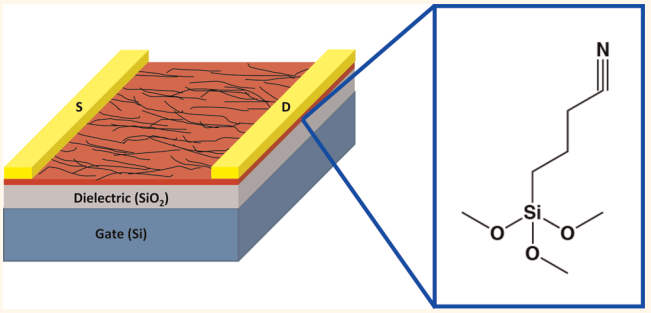

Amine-terminated self-assembled monolayers (SAMs) can be utilized to selectively adsorb semiconducting single-walled carbon nanotubes (S-SWNTs), but are not ideal. Formation of these monolayer films from silanes can be dramatically influenced by atmospheric and other processing conditions, resulting in poor-quality SAMs or irreproducible results. The surface sorting method of fabricating these semiconducting nanotube networks (SWNTnts) can become ineffective if the functionalized surface is not smooth with high amine density. However, by replacing the amine with a nitrile group, SAM formation can be made more controllable and reproducible. Upon SWNT deposition, the nitrile group was found to not only adsorb higher density SWNTnts but also sort the nanotubes efficiently, as shown by micro-Raman spectroscopy. Upon testing these SWNTnts for device performance, these thin-film transistors (TFTs) were also found to yield higher quality devices than those fabricated on amine surfaces. Overall, these results expand the applicability of surface sorting and SWNT adsorption to other organic functionalities for nanotube separation. This report provides an outline of the merits and characterization of using the nitrile functional group for the separation and adsorption of SWNTs and its integration in network TFTs.

KEYWORDS: self-assembled monolayer · carbon nanotubes · nanotube network · nanotube adsorption

Single-walled carbon nanotubes (SWNTs) are among the ever-growing list of nanoelectronic materials being studied that have shown the most promise in terms of real potential for device integration. These materials can be integrated into a variety of emerging technologies, including flexible electronics,[1−3] chemical/biological sensors,[4−9] active materials in electronic devices,[10,11] and photovoltaics.[12,13] To fully integrate into any of these desired applications, the carbon nanotubes need to be separated from their as-synthesized mixtures. When grown, nanotube films are a mixture of semiconducting (S-) and metallic (M-) SWNTs. Network films are required because the standalone S-SWNT devices are not practical to fabricate, despite yielding impressive device performance.[14,15] The resulting chirality mixture network must be sorted to be integrated into any usable application. A variety of techniques have been developed to perform this sorting, including density gradient ultracentrifugation,[16] selective sidewall functionalization to suppress metallic conductivity,[17,18] electrical breakdown of metallic tubes,[19] polymer wrapping,[20] gel separation,[21] and solution dispersion and separation.[22,23] However, large-scale separation remains challenging.

We recently developed a technique known as surface-sorting that utilized noncovalent interactions between organic functional groups confined to surfaces and SWNTs.[24,25] Previous reports had suggested that amines preferentially interact with S-SWNTs,[23,26−31] whereas aromatic groups preferred to adsorb to M-SWNTs.[32−34] By depositing the nanotubes from solution onto surfaces functionalized with organic molecules while operating under a dynamic spin assembly, the SWNTs could be separated with a fairly high efficiency. In a single step, the SWNTs could be deposited, aligned, and sorted, with devices ready after electrode deposition. The amine self-assembled monolayer (SAM) used was the standard 3-aminopropyltriethoxysilane (APTES) with a static contact angle of 60−70°. The resulting semiconducting networks had impressive device characteristics: hole mobilities ranging from 0.5 to 6 $cm^2 V^{-1} s^{-1}$, ON/OFF current ratios between

* Address correspondence to zbao@stanford.edu.

Received for review January 10, 2012 and accepted May 3, 2012.

Published online May 15, 2012
10.1021/nn300124y

10^4 and 10^6, and a threshold voltage around +1 V. It was later found that the amine lone pair was responsible for the adsorption, donating some of its electron density to the SWNTs,[28,35,36] in contrast to some previous studies.[29,30]

Unfortunately, APTES, or amine silanes in general, are extremely sensitive to atmospheric and preparation conditions. This sensitivity can lead to difficulty in producing complete monolayers consistently and reproducibly. Whereas the maximum static contact angle for a full, dry amine surface is approximately 65°,[37] various reports have claimed complete films yield contact angles less than 10°, as low as 20°, as high as 93°, and everything in between.[31,38,39] Likewise, reported values for ellipsometric thicknesses vary wildly among these same reports, while a true monolayer should be approximately 9 Å.[37] Typical reasons for these wildly varying reports are the fact that amine silanes can noncovalently adsorb to the surface, blocking actual covalent reactions and leaving exposed silica upon deadsorption.[37,40] This can lead to low contact angles and submonolayer thicknesses. Amine silanes are also self-catalyzing given that the amine can slightly chelate to the silicon and form a highly reactive pentacoordinate complex.[41,42] Exposure to even minimal quantities of water or heat can lead to high levels of polymerization that will yield rough or multilayer surfaces.[39] These rough or polymerized surfaces can produce overly thick, hydrophobic films. For these reasons, for precise control over film growth, amine silanes must be reacted in dry environments for specific reaction times at specific temperatures and specific silane concentrations. The ultrasensitivity of these silanes to reaction conditions leads to extreme difficulty in forming true monolayers. Without a complete monolayer, the surface sorting technique becomes ineffective and poor enrichment of S-SWNTs adsorb to the surface. Finally, previous work has suggested that the electron density on the amine lone pair can transfer charge to SWNTs. This can have the detrimental effect of reducing the charge-carrying capacity of p-doped SWNTs in air, effectively dedoping the network.[28]

In this work, we examine an alternate functional group system to produce S-SWNT-rich network devices. Silanes terminated with the nitrile functional group are found to form satisfactory thin films consistently and reproducibly and have been found previously to interact strongly with S-SWNTs.[30,43] We examined the ability of these nitrile surfaces to adsorb SWNTnts and the quality of the resulting fabricated thin film transistors (TFTs). These films are then compared to similar networks on amine surfaces to determine if one functionalized surface is superior to the other when used for SWNTnts.

RESULTS AND DISCUSSION

SAM Formation. Silicon substrates with both native and 300 nm oxide films were modified with 11-cyanoundecyltrimethoxysilane (CUTS) in toluene at room temperature in air for 3 h. The resulting surfaces had a thickness of approximately 16.9 ± 0.6 Å, a static contact angle of 65.1° ± 2.5°, and rms roughness of 0.2 nm. See Figure 1 for silane structure and AFM surface topography. To examine the effect of humidity on SAM deposition, surface modifications were also completed in a nitrogen glovebox, yielding indistinguishable results. Reaction times of 1, 3, 6, 12, and 24 h were examined; however film thickness and contact angles varied negligibly after 3 h. At 1 h, the monolayer thickness was slightly reduced but cannot be validated at 95% confidence. On average, the contact angle was approximately 5° lower for the 1 h reactions as compared to the 3 h reactions. In contrast, the standard amine SAM (3-aminopropyltriethoxysilane, APTES) is highly reactive to water and requires use of a dry atmosphere to prevent the formation of multilayers. Also silane purity is essential for proper monolayer formation, so vacuum distillation is required before using APTES. The nitrile SAM, CUTS, did not require distillation and produced smooth monolayers without much difficulty.

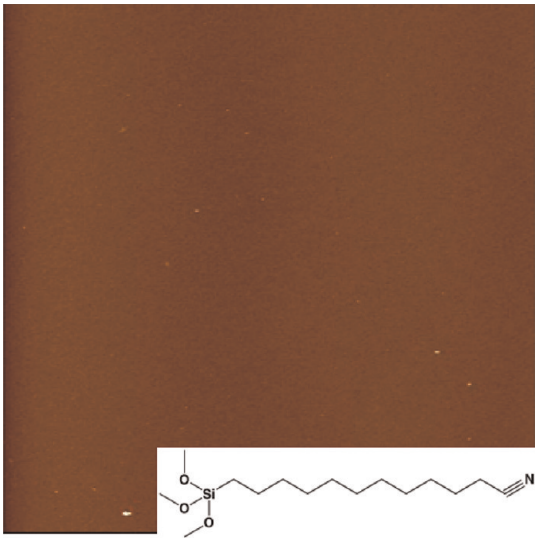

Figure 1. 10 × 10 μm^2 AFM topography of SiO_2 coated with nitrile SAM. rms roughness = 0.2 nm. *z*-scale = 5 nm. Inset: Structure of 11-cyanoundecyltrimethoxysilane (CUTS).

SWNT Network Formation. After surface modification, solutions of arc-discharge SWNTs dispersed in *N*-methylpyrrolidone (NMP) at a concentration of 5 μg/mL were spun-cast on these substrates at various spin rates. For the APTES surface, 4k rpm was found to be the ideal spin speed for sorting and proper SWNTnt density, moderate alignment, and excellent TFT characteristics.[24,25] Using this spin speed as a benchmark, a preliminary comparison could be made with the nitrile surface based solely on SWNT adsorption. It should be noted that in this work a more dilute 5 μg/mL solution was used (as opposed to the 10 μg/mL used by LeMieux *et al.*)[24,25] to limit the presence and adsorption of bundles. The optimal concentration typically depends on the batch of SWNTs used.

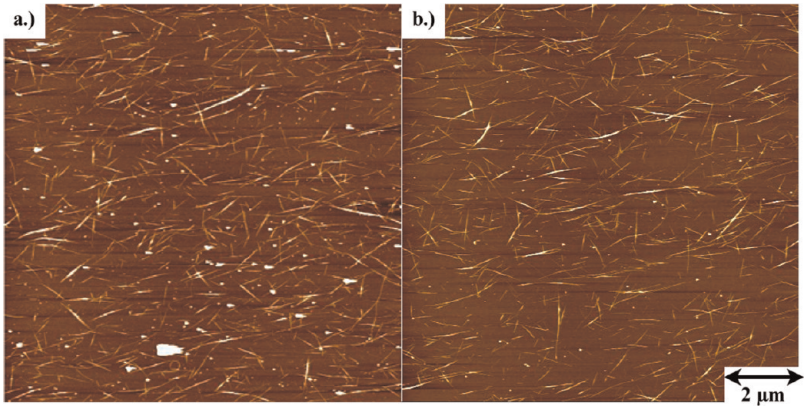

Figure 2. Comparison of high density SWNTnt on (a) nitrile surface *vs* (b) amine surface. Deposition conditions: 150 μL of a 10 μg/mL solution. SWNTnt density: ~20 SWNTs/μm^2. For similar deposition conditions on amine surfaces, this density is only 15 SWNTs/μm^2. *z*-scale = 10 nm.

To obtain a SWNTnt density of approximately 15 SWNTs/μm^2, the amine surface required 150 μL of a 10 μg/mL solution as compared to 200 μL of a 5 μg/mL on the nitrile surface. Fifty percent more raw nanotubes are required for deposition on the amines than on the nitriles. When the same depositions are used on both surfaces (150 μL of a 10 μg/mL solution), the nitrile surface adsorbs over 20 SWNTs/μm^2, whereas only approximately 15 SWNTs/μm^2 adsorb on the APTES surface[25] (Figure 2). These results suggested that SWNTs adsorb somewhat more strongly to the nitrile surfaces than the amine surfaces. Since individual nitriles and amines have been shown to interact with SWNTs with roughly the same interaction energy,[30,43] the adsorption differences are likely related to the SAM density. The longer alkyl chain on the nitrile SAM used could pack more efficiently, and hence higher nitrile surface density could be obtained.[44,45] The short-chain amine, APTES, cannot pack as well, and fewer amines were likely to exist in a monolayer. This claim could not be validated by XPS because of low amine intensity. A long-chain amine (such as 11-aminoundecyltriethoxysilane) could not be used for comparison because the silane polymerized too quickly in all conditions and a smooth monolayer could not be obtained.

To optimize the deposition conditions specifically for the nitrile surface, various spin speeds and deposition volumes were considered. Initially the volume was kept constant for varying spin speeds. In Figure 3, the 2k, 4k, 6k, and 8k rpm spin speeds are shown. Higher spin speeds were not examined because the network density was too low for subsequent analysis. At low spin speeds, such as 2k rpm, the SWNTnt has a very high density, high bundle density, and low alignment. At this spin speed the shear flow is not strong enough to segregate the SWNTs before they fully adsorb to the surface. The slow spin rate likewise limits the alignment of the nanotubes while in solution or when initially touching down on the surface. At higher spin speeds, the network has noticeably higher alignment, since the flow could more quickly align the SWNTs before touching the surface. Also, the decreasing density is an artifact of the higher flow rates washing more nanotubes away before they can adsorb.

When the solution volume was varied to fabricate samples of varying spin speed, but constant SWNTnt density, μRaman analysis shows there is a clear enhancement of S-SWNT adsorption. Figure 4 compares the radial breathing modes (RBMs), D-band, and G-band regions of the Raman spectra of samples spun at 1k through 8k rpm. For the 633 nm (1.96 eV) excitation energy and for AD-CNTs, the cutoff between the E^S_{33} and E^M_{11} transitions is at approximately 178 cm^{-1}.[46,47] Lower energy transitions in the spectra corresponded to S-SWNTs, and higher energies to M-SWNTs. All data are referenced to the 172 cm^{-1} peak, which corresponded to the average diameter of the AD-CNTs. There is a distinct shoulder in the metallic region for all spin speeds; however there is a gradual reduction in intensity. For slower spin speeds, 1k−3k, the shoulder is slightly more intense, where the flow rate was likely too low to adequately sort the SWNTs during adsorption. For all higher spin speeds, 4k and above, there was a non-negligible reduction in the metallic shoulder intensity, with the greatest reduction at the 8k spin speed, giving evidence of increased sorting. See the Supporting Information for corroborating RBM data at 532 nm laser excitation. The G-bands showed no trend with spin speed, and the D/G intensity ratio was relatively constant at approximately 0.18 ± 0.02.

SWNTntTFT Performance. To confirm the trends in sorting, Au electrodes were deposited, and the resulting devices were tested. Two sets of data were collected: samples deposited with constant solution volume and samples with equal SWNTnt density. Figure 5 displays composite average transfer curves comparing the 2k, 4k, 6k, and 8k rpm samples fabricated from deposition of 200 μL of a 5 μg/mL solution. All devices were operated in the linear regime at a drain voltage of −0.5 V on 300 nm SiO_2 with channel

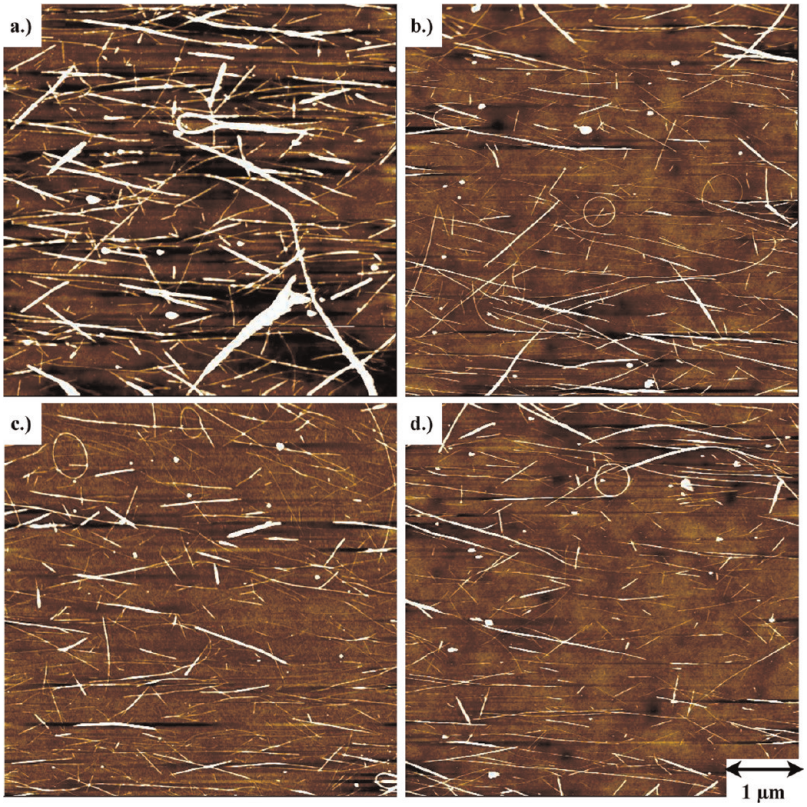

Figure 3. Comparison of SWNTnt density at varying spin speeds: (a) 2k rpm; (b) 4k rpm; (c) 6k rpm; (d) 8k rpm. Note the decreasing density and increasing alignment with increasing spin speed, as expected.[25] 200 μL of a 5 μg/mL ADCNT/NMP solution was deposited. *z*-scale = 5 nm.

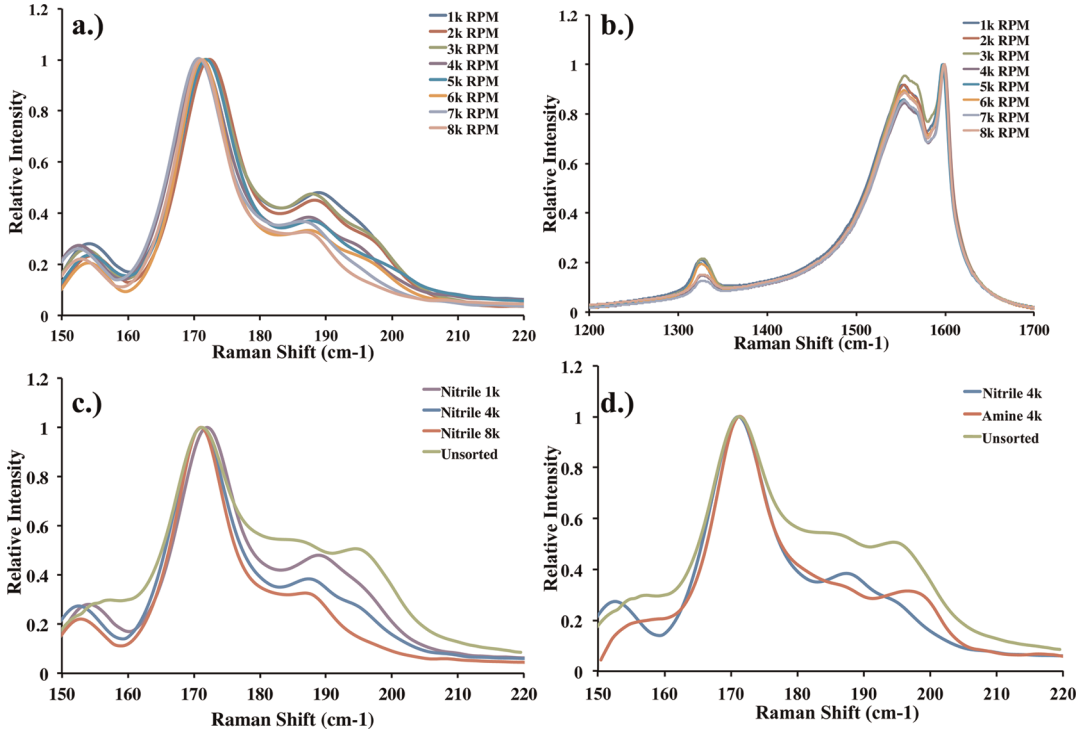

Figure 4. μRaman analysis of ~15 SWNT/μm^2 density SWNTnts on nitrile surfaces at varying spin speed. (a) RBM region. Note the increased metallic shoulder for 1k−3k rpm. For 4k and above, there is a distinct decrease in this shoulder, with the smallest shoulder for the 8k rpm spin speed. (b) G-band region. There is no noticeable trend in the D- or G-bands with spin speed.

W/L = 20. Table 1 enumerates key device parameters. Clearly, the unsorted, high-density networks on the 2k rpm samples resulted in high operating and leakage currents, with a subsequently low ON/OFF current ratio. For increasing speeds, the network densities decreased, leading to decreasing ON currents, decreasing OFF currents, decreasing mobilities, and increasing ON/OFF current ratios. The threshold voltage was relatively constant, ranging between −1 and −2 V, which is approximately 2−3 V lower than similar devices on APTES surfaces. Typical output curves, hysteresis curves, and transfer curves with 95% confidence intervals are included in the Supporting Information.

To better examine the effectiveness of sorting on the nitrile surfaces, devices with constant SWNTnt density (approximately 13 SWNT/μm^2) were fabricated. Since increasing the spin speed required greater volumes of solution, we were able to obtain working devices for higher spin speeds. It should be noted that the lower SWNTnt density was chosen to specifically reduce the 4k rpm OFF current, which was a benchmark spin speed standard to compare to the amine surfaces. Figure 6 displays composite average transfer curves comparing 2k−11k rpm samples, and Table 2 enumerates the key device parameters. The 2k rpm samples were clearly still not sorted as well as other samples. Despite having a constant network density like all other samples, the network contained more M-SWNTs and more bundles, increasing the current-carrying capacity of the network and reducing the threshold voltage (absolute value), but leading to high OFF currents. Sorting was slightly improved with a lower network density, as the ON/OFF ratio was increased by over an order of magnitude from the previous experiment. All other spin speeds yielded roughly equivalent devices. The threshold voltage of these samples was approximately 1−2 V lower than the previous data set, an artifact of the reduced network densities. Radial density gradients were observed for the higher spin rates, minimal for 8k, but fairly dramatic for 10k and 11k rpm. On the 8k rpm samples, the max ON current reduced to roughly 100 nA in the last few devices close to the substrate edge (approximately 1 cm from sample center). This was a result of the reduced network density. Within 3−4 mm from sample center on the 10k and 11k rpm samples, the ON current quickly dropped from ∼2 μA to ∼100 nA. Subsequently, the ON currents decreased further until devices became insulating, as the SWNTnt density decreased below the percolation threshold. Although not statistically significant (as shown in the Supporting Information), the 11k rpm samples yielded slightly higher ON currents and mobilities because devices had to be tested closer to the sample center, where sorting has been shown to be slightly less efficient.[24] Due to the high spin speed, the network was highly aligned but contained a larger than average density of bundles (see Supporting Information).

When comparing the SWNTnt devices fabricated on nitrile surfaces to those on amine surfaces, many clear differences were observed. As noted above, for a given volume of solution deposited, the nitrile surfaces

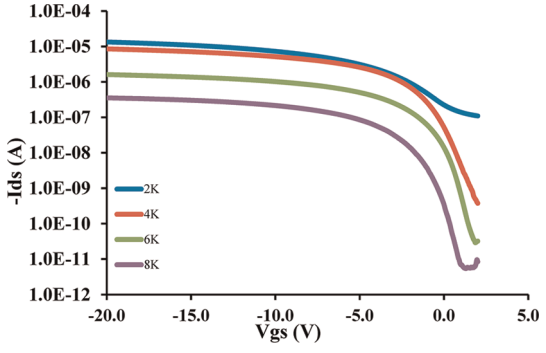

Figure 5. Transfer characteristics for SWNT solution deposited on nitrile surfaces at varying spin speeds. Volume deposited = 200 μL. V_{ds} = −0.5 V. Devices on 300 nm SiO_2.

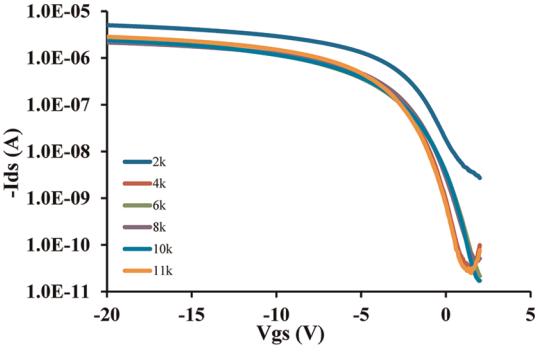

Figure 6. Transfer characteristics for SWNT solution deposited on nitrile surfaces for constant SWNTnt density. SWNTnt density = 13 SWNT/μm^2. V_{ds} = −0.5 V. Devices on 300 nm SiO_2.

TABLE 1. Transfer Characteristics for SWNTnts Deposited on Nitrile Surfaces[a]

spin speed (rpm)	SWNTNT density (μm^{-2})	ON/OFF current ratio	mobility (cm^2 V^{-1} s^{-1})	V_{th} (V)	ON current (μA)	OFF current
2k	19 ± 5[b]	122 ± 57	8.47 ± 1.74	−1.29 ± 0.49	13.4 ± 2.66	110 ± 50 nA
4k	15 ± 3	2.30(±1.01) × 10^4	6.40 ± 0.89	−0.95 ± 0.26	8.59 ± 1.29	378 ± 130 pA
6k	12 ± 2	5.52(±1.43) × 10^4	1.23 ± 0.23	−0.92 ± 0.30	1.62 ± 0.27	29.4 ± 8.9 pA
8k	8 ± 2	6.58(±1.10) × 10^4	0.28 ± 0.16	−1.96 ± 0.39	0.36 ± 0.09	5.42 ± 1.30 pA

[a] Constant SWNT solution deposition (200 μL of a 5 μg/mL solution) on 300 nm SiO_2. V_{ds} = −0.5 V. [b] The high density of bundles present at 2k rpm made accurate counting of SWNTs difficult, leading to relatively high variation between samples.

TABLE 2. Transfer Characteristics for SWNTnts Deposited on Nitrile Surfaces[a]

spin speed (rpm)	volume deposited (μL)	ON/OFF current ratio	mobility (cm^2 V^{-1} s^{-1})	V_{th} (V)	ON current (μA)	OFF current
2k	150	$1.90(\pm1.26) \times 10^3$	3.69 ± 1.31	-1.42 ± 0.12	5.05 ± 1.04	271 ± 150 nA
4k	200	$6.74(\pm2.26) \times 10^4$	1.64 ± 0.46	-2.41 ± 0.38	2.35 ± 0.63	34.8 ± 7.8 pA
6k	250	$1.20(\pm0.47) \times 10^5$	1.67 ± 0.33	-2.91 ± 0.16	2.58 ± 0.49	21.5 ± 11.7 pA
8k	300	$4.73(\pm2.64) \times 10^4$	1.64 ± 0.36	-2.10 ± 0.29	2.16 ± 0.52	45.6 ± 23.3 pA
10k	350	$1.41(\pm0.50) \times 10^5$	1.60 ± 0.23	-2.69 ± 0.17	2.41 ± 0.33	17.1 ± 5.6 pA
11k	375	$1.13(\pm0.44) \times 10^5$	2.12 ± 0.54	-2.74 ± 0.24	2.85 ± 0.62	25.2 ± 8.9 pA

[a] Constant SWNTnt density (13 SWNT/μm^2 from a 4.5 μg/mL solution) on 300 nm SiO_2. $V_{ds} = -0.5$ V.

adsorb higher densities of SWNTs compared to the amine surface. For a given SWNT density however, the nitrile surfaces also seem to offer device performance improvements over the amine surfaces. When comparing devices on both surfaces at the same V_d and $V_g - V_{th}$, similar ON currents and ON/OFF ratios were observed. Higher ON currents are reported here (compared to previous studies[24,25]) because V_g was swept to higher voltages, producing a $2-3\times$ increase in current. The hole mobilities of the devices on each surface were also comparable, with slightly higher mobilities being observed on the amine surfaces. This was likely an artifact of the reduced density of the SWNTnt on the nitrile surface, as shown in Figure 6 and Table 2. Comparing previous amine data[25] at 4k with SWNTnt density around 15 SWNT/μm^2 with that shown in Figure 5 and Table 1 on the nitrile surface suggests significantly higher mobilities can actually be obtained on the nitrile surfaces. It should be noted that although these mobilities seem relatively low compared to other developed methods, coupled with their high ON/OFF current ratios, these devices yield results on par with or better than other published techniques.[48,49]

The most significant difference between the two surfaces was the approximately 4 V decrease in the threshold voltage on the nitrile surface as compared to the amine. This can be a result of a combination of effects: altered electron density donation/withdrawal by the nitrogen lone pair, a significantly different dipole moment between the functional groups, and/or the presence of surface charges. Amine surfaces are known to donate some electron density from the lone pair to SWNTs, which ultimately alters the charge carrier density in the p-type (when in air) devices,[28,50] but the nitrogen lone pair on the nitrile surface is less electron-donating and would be expected to have the opposite effect. If this effect were dominant, the nitrile surface would be expected to make the network devices easier to turn on and, hence, have an increased V_{th}, as a sign of operating deeper in the device accumulation mode. The opposite effect is seen, however. This suggests the dipole effect mentioned above may play a larger role. With the difference in the electron density distribution between the amine and nitrile functionalities, the nitrile functional group is significantly more polar than the amine. Indeed, the local dipole moment of the lone nitrile functionality is greater in magnitude than the amine. This dipole moment can produce an electric field that opposes the gate field, making the network devices more difficult to turn on, operating in depletion mode, and potentially shifting the V_{th} to negative values. Similar threshold voltage shifts have been observed for this reason in previous work.[51] Another important effect could be the induced dipole by the presence of surface charges on the SAM layers. Amines can attract water and form ammonium ions much easier than nitriles becoming protonated. These ions can induce surface dipoles and have been shown to drive the threshold voltage to relatively large positive values.[35,36,52] Also, the ammonium ion is prevented from donating electron density to the SWNT, subsequently making the device easier to turn on while on amine surfaces.

CONCLUSIONS

In summary, we have shown in previous reports that high-quality SWNTnt TFTs can be fabricated by exploiting the SWNT interactions with the amine functional group. The most crucial and most difficult step in this fabrication is obtaining the amine-functionalized SAM monolayer. Amine silanes are unpredictable, at best, and without the confidence of producing a clean, reproducible monolayer, the surface sorting technique would be limited. We have shown in this report that the nitrile functionality serves as a satisfactory replacement for the amine. Not only is the SAM formation more predictable and reproducible, but SWNTs interact very strongly with nitrile groups. Nitrile-coated surfaces adsorb SWNTnts with greater densities, higher current-carrying capacity, and lower threshold voltages. The amine group can donate electron density and charge to the SWNTs, effectively dedoping them and reducing their performance. The nitrile group, on the other hand, with reduced electron donation ability, can adsorb to the SWNTs strongly without reducing the air-induced p-type doping. As a consequence, the surface sorting technique has a greater opportunity of being implemented in large-scale SWNTnt device fabrication. Ease of processing and

enhanced device performance suggests that the nitrile functionality holds the promise of bringing air-stable, solution-processed SWNTnts into greater presence in household electronic devices.

EXPERIMENTAL SECTION

Surface Modification. Surface modification experiments were performed using both native and thermally grown, 300 nm, oxide on heavily n-doped Si(100) wafers (Silicon Quest). All substrates were held in a glass staining jar and cleaned for 30 min in a piranha bath (3:1 H_2SO_4/H_2O_2; *caution: highly reactive toward organics*). They were subsequently rinsed and sonicated in deionized water for another 30 min. Samples were then dried under N_2 and prepared for silane modification. The nitrile-capped silane used was 11-cyanoundecyltrimethoxysilane and was purchased from Gelest. The reaction can take place in a nitrogen glovebox or in air. The substrates were submerged in a 0.4% by volume solution of silane in anhydrous toluene (in glovebox) or HPLC grade toluene (outside the glovebox) for 1−6 h. Insignificant changes were observed for longer than 3 h of reaction. Following the surface modification, they were rinsed repeatedly with clean anhydrous toluene, sonicated, rinsed again in toluene, then dried under N_2, and annealed under vacuum for 20 min at 100 °C before characterization. SAM surface roughness ranged from 0.1 to 0.3 nm.

Nanotube Solution Preparation. Details of the nanotube purification and dispersion are provided in a previous publication.[24] A 80 mg amount of arc-dishcarged single-walled nanotubes (AD-SWNTs) obtained from ILJIN Nanotech, grade ASP-100F, and 2 g of sodium dodecyl sulfate (SDS), from J.T. Baker, were mixed with 200 mL of Ultrapure water (0.1 m filtered, from Invitrogen). The mixture was sonicated in a Cole-Palmer Ultrasonic Processor at 750 W and 100% amplitude for 30 min in an ice/water bath. The sonicated mixture was centrifuged using a Sorvall RC5C Plus centrifuge at 12 500 rpm for 4 h at 4 °C. Approximately 80% of the supernatant was decanted and diluted with anhydrous acetone to dissociate the SDS from the SWNTs. The flocculated SWNTs were collected by centrifugation and rinsed several times with acetone to completely remove SDS. The suspension was filtered through a PTFE membrane (Millipore, 0.45 μm pore size) to collect the nanotubes as a "bucky paper". This was peeled off the membrane, dried under vacuum overnight at 50 °C, and stored in a desiccator. Nanotube solutions were produced by dissolving the bucky paper (by 20 min of ultrasonication at 700 W, 60% amplitude) at a concentration of 4−5 μg/mL in NMP (Omnisolve, spectrophotometry grade).

SWNT Deposition. The CNT solution was carefully dropped *via* 1 mL syringe using a syringe pump near the surface in the center of a 2.5 cm × 1.5 cm modified Si wafer spinning at speeds ranging from 1k to 11k rpm (Headway Research). The solution was deposited at a rate of 1.7 mL/h, which roughly corresponded for the given syringe and needle to approximately 1 drop every 10 s. Volumes deposited varied by experiment, as noted in the text.

Sample Characterization. AFM topography images were acquired in the tapping mode regime using a Multimode AFM (Veeco). Images were taken at approximately the same location on each sample. Density and length analyses were carried out using Image J software (NIH). μ-Raman (LabRam Aramis, Horiba Jobin Yvon) measurements were carried out at 633 nm (1.96 eV) at 100× magnification with 1 μm spot size and 1200 grating. Excitation power through the filter was 2 mW. All data were acquired from automated multipoint (9−12 points) mapping over random regions on the samples (except the unsorted sample center), with three spectra accumulated and averaged at each single point. Approximately 8−10 mapping locations were chosen, yielding scans on each sample performed at spacings of approximately 50−100 μm. All summarized RBM data were normalized to the intensity of the dominant RBM peak, at 172 cm^{-1}, and all summarized G-band data were normalized to the intensity of the G^+-band at 1592 cm^{-1}.

Device Fabrication and Testing. Transistor devices were made *via* thermal evaporation of gold electrodes (40 nm) through a shadow mask placed on the SWNT-coated substrates. The resultant devices had channels of 50 μm length and 1 mm width. Electrical characterization was performed using a Keithley 4200 SC semiconductor parameter analyzer. Capacitance was determined using a simple parallel plate model (since the more rigorous model accounting for capacitance coupling of SWNTs was found to yield a similar value), and mobility was determined using the simple linear transistor equation.

Conflict of Interest: The authors declare no competing financial interest.

Acknowledgment. This research was supported by the National Science Foundation (NSF) ECCS 0901414 and Stanford Global Climate & Energy Program (GCEP). J.P.O. acknowledges support from the Stanford Graduate Fellowship (SGF). M.C.L. thanks the IC postdoctoral fellowship for support. Z.B. acknowledges support from a Sloan Research Fellowship.

Supporting Information Available: Alternate device characteristics, statistical error in transfer curves for networks with constant nanotube density, and topographical comparison of nanotube alignment at varying spin speeds. This material is available free of charge *via* the Internet at http://pubs.acs.org.

REFERENCES AND NOTES

1. Ahn, J.-H.; Kim, H.-S.; Lee, K. J.; Jeon, S.; Kang, S. J.; Sun, Y.; Nuzzo, R. G.; Rogers, J. A. Heterogeneous Three-Dimensional Electronics by Use of Printed Semiconductor Nanomaterials. *Science* **2006**, *314*, 1754–1757.
2. Grüner, G. Carbon Nanotube Films for Transparent and Plastic Electronics. *J. Mater. Chem.* **2006**, *16*, 3533–3539.
3. Hellstrom, S.; Lee, H.; Bao, Z. Polymer-Assisted Direct Deposition of Uniform Carbon Nanotube Bundle Networks for High Performance Transparent Electrodes. *ACS Nano* **2009**, *3*, 1423–1430.
4. Snow, E. S.; Perkins, F. K.; Robinson, J. A. Chemical Vapor Detection Using Single-Walled Carbon Nanotubes. *Chem. Soc. Rev.* **2006**, *35*, 790.
5. Barone, P. W.; Parker, R. S.; Strano, M. S. *In Vivo* Fluorescence Detection of Glucose Using a Single-Walled Carbon Nanotube Optical Sensor: Design, Fluorophore Properties, Advantages, and Disadvantages. *Anal. Chem.* **2005**, *77*, 7556–7562.
6. Kuzmych, O.; Allen, B. L.; Star, A. Carbon Nanotube Sensors for Exhaled Breath Components. *Nanotechnology* **2007**, *18*, 375502.
7. Star, A.; Han, T. R.; Joshi, V.; Gabriel, J. C. P.; Grüner, G. Nanoelectronic Carbon Dioxide Sensors. *Adv. Mater.* **2004**, *16*, 2049–2052.
8. Wang, F.; Gu, H.; Swager, T. M. Carbon Nanotube/Polythiophene Chemiresistive Sensors for Chemical Warfare Agents. *J. Am. Chem. Soc.* **2008**, *130*, 5392–5393.
9. Roberts, M. E.; Lemieux, M. C.; Bao, Z. Sorted and Aligned Single-Walled Carbon Nanotube Networks for Transistor-Based Aqueous Chemical Sensors. *ACS Nano* **2009**, *3*, 3287–3293.
10. Xue, W.; Liu, Y.; Cui, T. High-Mobility Transistors Based on Nanoassembled Carbon Nanotube Semiconducting Layer and SiO_2 Nanoparticle Dielectric Layer. *Appl. Phys. Lett.* **2006**, *89*, 163512.
11. Ryu, K.; Badmaev, A.; Wang, C.; Lin, A.; Patil, N.; Gomez, L.; Kumar, A.; Mitra, S.; Wong, H. S. P.; Zhou, C. CMOS-Analogous Wafer-Scale Nanotube-on-Insulator Approach for Submicrometer Devices and Integrated Circuits Using Aligned Nanotubes. *Nano Lett.* **2008**, *9*, 189–197.

12. Rowell, M. W.; Topinka, M. A.; Mcgehee, M. D.; Prall, H.-J.; Dennler, G.; Sariciftci, N. S.; Hu, L.; Gruner, G. Organic Solar Cells with Carbon Nanotube Network Electrodes. *Appl. Phys. Lett.* **2006**, *88*, 233506.
13. Li, C.; Chen, Y.; Wang, Y.; Iqbal, Z.; Chhowalla, M.; Mitra, S. A Fullerene/Single Wall Carbon Nanotube Complex for Polymer Bulk Heterojunction Photovoltaic Cells. *J. Mater. Chem.* **2007**, *17*, 2406–2411.
14. Fuhrer, M.; Kim, B.; Dürkop, T. High-Mobility Nanotube Transistor Memory. *Nano Lett.* **2002**, *2*, 755–759.
15. Dürkop, T.; Getty, S.; Cobas, E.; Fuhrer, M. Extraordinary Mobility in Semiconducting Carbon Nanotubes. *Nano Lett.* **2004**, *4*, 35–39.
16. Arnold, M. S.; Green, A. A.; Hulvat, J. F.; Stupp, S. I.; Hersam, M. C. Sorting Carbon Nanotubes by Electronic Structure Using Density Differentiation. *Nat. Nanotechnol.* **2006**, *1*, 60–65.
17. Kanungo, M.; Lu, H.; Malliaras, G.; Blanchet, G. Suppression of Metallic Conductivity of Single-Walled Carbon Nanotubes by Cycloaddition Reactions. *Science* **2009**, *323*, 234.
18. Strano, M. S. Electronic Structure Control of Single-Walled Carbon Nanotube Functionalization. *Science* **2003**, *301*, 1519–1522.
19. Collins, P. G.; Arnold, M.; Avouris, P. Engineering Carbon Nanotubes and Nanotube Circuits Using Electrical Breakdown. *Science* **2001**, *292*, 706–709.
20. Yi, W.; Malkovskiy, A.; Chu, Q.; Sokolov, A. P.; Colon, M. L.; Meador, M.; Pang, Y. Wrapping of Single-Walled Carbon Nanotubes by a π-Conjugated Polymer: The Role of Polymer Conformation-Controlled Size Selectivity. *J. Phys. Chem. B* **2008**, *112*, 12263–12269.
21. Miyata, Y.; Shiozawa, K.; Asada, Y.; Ohno, Y.; Kitaura, R.; Mizutani, T.; Shinohara, H. Length-Sorted Semiconducting Carbon Nanotubes for High-Mobility Thin Film Transistors. *Nano Res.* **2011**, *4*, 963–970.
22. Zheng, M.; Jagota, A.; Semke, E. D.; Diner, B. A.; Mclean, R. S.; Lustig, S. R.; Richardson, R. E.; Tassi, N. G. DNA-Assisted Dispersion and Separation of Carbon Nanotubes. *Nat. Mater.* **2003**, *2*, 338–342.
23. Chattopadhyay, D.; Galeska, I.; Papadimitrakopoulos, F. A Route for Bulk Separation of Semiconducting from Metallic Single-Wall Carbon Nanotubes. *J. Am. Chem. Soc.* **2003**, *125*, 3370–3375.
24. Lemieux, M. C.; Roberts, M.; Barman, S.; Jin, Y. W.; Kim, J. M.; Bao, Z. Self-Sorted, Aligned Nanotube Networks for Thin-Film Transistors. *Science* **2008**, *321*, 101–104.
25. LeMieux, M.; Sok, S.; Roberts, M.; Opatkiewicz, J.; Liu, D.; Barman, S.; Patil, N.; Mitra, S.; Bao, Z. Solution Assembly of Organized Carbon Nanotube Networks for Thin-Film Transistors. *ACS Nano* **2009**, *3*, 4089–4097.
26. Lu, J.; Lai, L.; Luo, G.; Zhou, J.; Qin, R.; Wang, D.; Wang, L.; Mei, W. N.; Li, G.; Gao, Z.; *et al*. Why Semiconducting Single-Walled Carbon Nanotubes Are Separated from their Metallic Counterparts. *Small* **2007**, *3*, 1566–1576.
27. Basiuk, E. V.; Basiuk, V. A.; Bañuelos, J.-G.; Saniger-Blesa, J.-M.; Pokrovskiy, V. A.; Gromovoy, T. Y.; Mischanchuk, A. V.; Mischanchuk, B. G. Interaction of Oxidized Single-Walled Carbon Nanotubes with Vaporous Aliphatic Amines. *J. Phys. Chem. B* **2002**, *106*, 1588–1597.
28. Kong, J.; Dai, H. Full and Modulated Chemical Gating of Individual Carbon Nanotubes by Organic Amine Compounds. *J. Phys. Chem. B* **2001**, *105*, 2890–2893.
29. Maeda, Y.; Kimura, S.; Kanda, M.; Hirashima, Y.; Hasegawa, T.; Wakahara, T.; Lian, Y.; Nakahodo, T.; Tsuchiya, T.; Akasaka, T. Large-Scale Separation of Metallic and Semiconducting Single-Walled Carbon Nanotubes. *J. Am. Chem. Soc.* **2005**, *127*, 10287–10290.
30. Friddle, R. W.; Lemieux, M. C.; Cicero, G.; Artyukhin, A. B.; Tsukruk, V. V.; Grossman, J. C.; Galli, G.; Noy, A. Single Functional Group Interactions with Individual Carbon Nanotubes. *Nat. Nanotechnol.* **2007**, *2*, 692–697.
31. Burgin, T.; Lewenstein, J.; Werho, D. Investigations into the Mechanism of Adsorption of Carbon Nanotubes onto Aminopropylsiloxane Functionalized Surfaces. *Langmuir* **2005**, *21*, 6596–6602.
32. Gotovac, S.; Honda, H.; Hattori, Y.; Takahashi, K.; Kanoh, H.; Kaneko, K. Effect of Nanoscale Curvature of Single-Walled Carbon Nanotubes on Adsorption of Polycyclic Aromatic Hydrocarbons. *Nano Lett.* **2007**, *7*, 583–587.
33. Star, A.; Han, T.; Gabriel, J.; Bradley, K.; Grüner, G. Interaction of Aromatic Compounds with Carbon Nanotubes: Correlation to the Hammett Parameter of the Substituent and Measured Carbon Nanotube FET Response. *Nano Lett.* **2003**, *3*, 1421–1423.
34. Zhao, J.; Lu, J.; Han, J.; Yang, C. Noncovalent Functionalization of Carbon Nanotubes by Aromatic Organic Molecules. *Appl. Phys. Lett.* **2003**, *82*, 3746–3748.
35. Opatkiewicz, J.; LeMieux, M.; Bao, Z. Influence of Electrostatic Interactions on Spin-Assembled Single-Walled Carbon Nanotube Networks on Amine-Functionalized Surfaces. *ACS Nano* **2010**, *4*, 1167–1177.
36. Opatkiewicz, J. P.; Lemieux, M. C.; Patil, N. P.; Wei, H.; Mitra, S.; Bao, Z. The Effect of Amine Protonation on the Electrical Properties of Spin-Assembled Single-Walled Carbon Nanotube Networks. *Nanotechnology* **2011**, *22*, 125201.
37. Smith, E. A.; Chen, W. How To Prevent the Loss of Surface Functionality Derived from Aminosilanes. *Langmuir* **2008**, *24*, 12405–12409.
38. Petri, D.; Wenz, G.; Schunk, P.; Schimmel, T. An Improved Method for the Assembly of Amino-Terminated Monolayers on SiO_2 and the Vapor Deposition of Gold Layers. *Langmuir* **1999**, *15*, 4520–4523.
39. Howarter, J.; Youngblood, J. Optimization of Silica Silanization by 3-Aminopropyltriethoxysilane. *Langmuir* **2006**, *22*, 11142–11147.
40. Kanan, S.; Tze, W.; Tripp, C. Method to Double the Surface Concentration and Control the Orientation of Adsorbed (3-Aminopropyl) dimethylethoxysilane on Silica Powders and Glass Slides. *Langmuir* **2002**, *18*, 6623–6627.
41. Blitz, J. P.; Shreedhara Murthy, R. S. Leyden, D. S. Ammonia-Catalyzed Silylation Reactions of Cab-O-Sil with Methoxymethylsilanes. *J. Am. Chem. Soc.* **1987**, *109*, 7141–7145.
42. Kinkel, J. N.; Unger, K. K. Role of Solvent and Base in the Silanization Reaction of Silicas for Reversed-Phase High-Performance Liquid Chromatography. *J. Chromatogr. A* **1984**, *316*, 193–200.
43. Cicero, G.; Grossmann, J.; Galli, G. Adhesion of Single Functional Groups to Individual Carbon Nanotubes: Electronic Effects Probed by *ab Initio* Calculations. *Phys. Rev. B* **2006**, *74*, 035425.
44. Porter, M. D.; Bright, T. B.; Allara, D. L.; Chidsey, C. E. D. Spontaneously Organized Molecular Assemblies. 4. Structural Characterization of n-Alkyl Thiol Monolayers on Gold by Optical Ellipsometry, Infrared Spectroscopy, and Electrochemistry. *J. Am. Chem. Soc.* **1987**, *109*, 3559–3568.
45. Evans, S.; Sharma, R.; Ulman, A. Contact Angle Stability: Reorganization of Monolayer Surfaces? *Langmuir* **1991**, *7*, 156–161.
46. Dresselhaus, M.; Dresselhaus, G.; Jorio, A.; Souza Filho, A.; Saito, R. Raman Spectroscopy on Isolated Single Wall Carbon Nanotubes. *Carbon* **2002**, *40*, 2043–2061.
47. Jorio, A.; Saito, R.; Hafner, J.; Lieber, C.; Hunter, M.; Mcclure, T.; Dresselhaus, G.; Dresselhaus, M. Structural (n, m) Determination of Isolated Single-Wall Carbon Nanotubes by Resonant Raman Scattering. *Phys. Rev. Lett.* **2001**, *86*, 1118–1121.
48. Rouhi, N.; Jain, D.; Zand, K.; Burke, P. J. Fundamental Limits on the Mobility of Nanotube-Based Semiconducting Inks. *Adv. Mater.* **2010**, *23*, 94–99.
49. Rouhi, N.; Jain, D.; Burke, P. J. High-Performance Semiconducting Nanotube Inks: Progress and Prospects. *ACS Nano* **2011**, *5*, 8471–8487.
50. Shim, M.; Javey, A.; Kam, N. W. S.; Dai, H. Polymer Functionalization for Air-Stable N-Type Carbon Nanotube Field-Effect Transistors. *J. Am. Chem. Soc.* **2001**, *123*, 11512–11513.
51. Vosgueritchian, M.; Lemieux, M. C.; Dodge, D.; Bao, Z. Effect of Surface Chemistry on Electronic Properties of Carbon

Nanotube Network Thin Film Transistors. *ACS Nano* **2010**, *4*, 6137–6145.
52. Dezieck, A.; Acton, O.; Leong, K.; Oren, E. E.; Ma, H.; Tamerler, C.; Sarikaya, M.; Jen, A. K.-Y. Threshold Voltage Control in Organic Thin Film Transistors with Dielectric Layer Modified by a Genetically Engineered Polypeptide. *Appl. Phys. Lett.* **2010**, *97*, 013307.